# Study on the Contact Ratio of Base Mat of Reactor Buildings Considering Nonlinear Soil-Structure Interaction Effects

S. Aihara, K. Atsumi, K. Ujiie, K. Emori, M. Odajima, K. Masuda
*Kajima Corporation, 2-1-1, Nishi-Shinjuku, Shinjuku-ku, Tokyo 160, Japan*

SUMMARY

The objective of this paper is to evaluate the nonlinear soil-structure interaction effects resulting from base mat uplift for static lateral loads. Nonlinear soil-structure interaction effects are modeled through the use of equivalent soil-structure interaction frictional and axial springs, which properties are determined by results of experimental data. It is assumed that normal stresses in compression and corresponding shear stresses, and friction, can occur in the area of contact between the embedded structure and soil. The remaining parts of the structure and soil are based on elastic analysis.

A two-dimensional finite element method with incremental loadings is applied. The substructuring technique is used to reduce computation time. The results of this method with respect to the contact ratio of the base mat are compared with the values obtained by static elastic calculation which is simply derived from an overturing moment and a vertical load of the structure.

Tentative conclusions can be drawn as follows: For moderate lateral loadings of 3 K, where K is the static seismic coefficient and corresponds to approximately 0.2 G in the Building Code, no large difference is observed between contact ratio by this concept and those by the static elastic calculation. For large lateral loadings of more than 4 K, a contact ratio of 80% is obtained by this concept whereas a corresponding value of 50% is obtained by static elastic calculation. The contact ratio of the base mat seems to be improved by this concept. The contact ratio becomes smaller when both lateral and vertical earthquake loads are considered, than that considering lateral earthquake loads only.

This analytical concept will be developed into dynamic problems, and then it will be possible to state whether or not this concept can represent a true alternative for the contact ratio of the base mat of a structure.

## 1. Introduction

In an earthquake-resistant design of a nuclear reactor building, the evaluation of the contact ratio of the base mat is necessary as one method of verifying the stability of the building. In the past, this contact ratio was obtained generally by using a technique similar to design of an independent base mat, assuming earth pressure deriving from dead weight (axial force) and overturning moment during earthquake to be of triangular distribution. However, this method (conventional method) has a tendency for the contact ratio to be evaluated as being lower than actual, since the elastic deformations of the structure and soil, and the friction between the side surface of the structure and the soil are not considered.

Focusing on this point and an analytical fundamental study (precise analysis method) for making an evaluation close to actual was carried out considering the contact ratio of the structure during earthquake by elastic deformations of the structure and the soil, and friction and nonlinearity between the structure and the soil.

## 2. Evaluation of contact ratio by precise analysis method

### 2.1 Features of precise analysis method

The differences between the conventional method and the precise analysis method are shown in Table 1. The features of the precise analysis method are the following two points:

(1) The elastic deformations of the structure and soil are considered.

(2) The frictional resistance of the side surface of the structure is considered.

Analysis was performed (1) by using an FEM model, and (2) by inserting nonlinear axial and frictional springs between the structure and soil.

### 2.2 Force transmission mechanism between structure and soil

At the contact surface between the structure and surrounding soil, there are cases when they are in contact and when they are separated, and the mechanisms of force transmission in both cases are as shown in Fig. 1.

At the time of contact the normal-direction force is transmitted as axial force, and the tangential direction force is transmitted as frictional force (shear force). The frictional force is dependent on axial force in the normal direction, and also is a force which changes to dynamic frictional resistance from static frictional resistance when exceeding a certain stress level. On the other hand, it may be considered that there is no transmission of force in either the normal direction or tangential direction when the structure and soil are separated.

Further, it is also necessary to consider permanent soil pressure between the underground walls and foundation mat. When the construction procedure is taken into account, it may be considered that after rock excavation the stress at the surface of rock has been relieved, and therefore, it is thought permanent soil pressure is produced by the dead weight of the structure and backfill soil after the construction and backfill.

### 2.3 Modeling

The structure and soil were modeled by two-dimensional finite elements, the contact surface between structure and soil was evaluated by nonlinear springs, and the interaction effect was expressed at the contact surface.

The springs, as shown in Fig. 2, were evaluated as axial spring in the direction normal to the contact surface, and frictional spring (shear spring) in the tangential direction.

2.3.1 Normal direction (axial spring)

The axial spring was idealized as a geometrically nonlinear spring having a strong rigidity at the time of contact and zero rigidity when separated. Separation was determined to exist when tensile force was produced in the axial spring, judging that the cohesion between soil and structure to be slight in the normal direction.

2.3.2 Tangential direction (frictional spring--shear spring)

According to experimental results, frictional resistance increases with increase in axial pressure. Hence in one-directional loading experiments, the static frictional resistance is fairly large compared with dynamic frictional resistance, but in cyclic dynamic loading tests, the difference between static and dynamic frictional resistance has tendency to be small. Therefore, the frictional spring was idealized as an elasto-plastic spring of bi-linear type with the sum of frictional resistance depending on axial pressure and cohesion as the yield point (Eq. (1)). And with axial spring in a tensile stress state rigidity was taken to be zero.

$$Qy = (C + \sigma v \cdot \tan \phi)Ae \quad \cdots\cdots\cdots\cdots\cdots\cdots\cdots\cdots (1)$$

Qy: yield frictional force

C: cohesion

$\sigma v$: axial stress

$\tan \phi$: coefficient of friction

$\phi$: angle of friction

Ae: control area

2.4 Computation of contact ratio of base mat

The flow of computation of the contact ratio of the base mat is shown in Fig. 3. After establishing the analytical conditions, first the analysis is performed for the vertical state of load (dead weight), and the spring force between the structure and soil is calculated. Next, the analysis for the ratio during earthquake is performed by the load increment method, and at this time, with regard to the axial and frictional springs, the changes in the conditions against the sum of the spring forces under vertical and earthquake loads are judged, and then further analysis is carried out. Finally the contact ratio of the base mat of the structure is evaluated from the state of separation of the axial spring at the bottom surface of the structure.

3. Analytical procedure

A two-dimensional static nonlinear analysis was performed, while the load increment method was applied as analysis technique. It should be noted that nonlinear parts were only the springs between the structure and the soil, and therefore, sub-structuring technique was adopted.

3.1 Load increment method

The analysis flow according to the load increment method is shown in Fig. 4. Vertical load analyses of the structure and backfill soil are first made and resultant stresses are evaluated to be as initial stresses. Next, lateral earthquake load is divided and stress analyses of the nonlinear parts only are repeated a number of times equal to the number of divisions. In case a change in the condition occurs at some step, computations of changes in rigidity and of unbalanced force are carried out. After completion of the repeated calculations, stress analysis of the linear part is performed.

3.2 Sub-structuring technique

Field of the analytical model are divided into the four parts of A, B, C and D as shown in Fig. 5. The parts A and B are elastic bodies, while C and D are connected by nonlinear springs. The relationship between force (F) and displacement (D) expressed in matrix form is as follows:

$$\begin{Bmatrix} F_A \\ F_B \\ F_C \\ F_D \end{Bmatrix} = \begin{bmatrix} K_{AA} & 0 & K_{AC} & 0 \\ 0 & K_{BB} & 0 & K_{BD} \\ K_{CA} & 0 & K_{CC} & K_{CD} \\ 0 & K_{DB} & K_{DC} & K_{DD} \end{bmatrix} \begin{Bmatrix} D_A \\ D_B \\ D_C \\ D_D \end{Bmatrix} \quad \cdots\cdots\cdots\cdots (2)$$

Taking note of the fact that nonlinear parts are only the C and D parts, the $D_A$ and $D_B$ of Eq. (2) are eliminated, and when rearranged:

$$\begin{Bmatrix} R_C \\ R_D \end{Bmatrix} = \begin{bmatrix} \widetilde{K_{CC}} & K_{CD} \\ K_{DC} & \widetilde{K_{DD}} \end{bmatrix} \begin{Bmatrix} D_C \\ D_D \end{Bmatrix} \quad \cdots\cdots\cdots\cdots\cdots\cdots (3)$$

where,

$$\begin{cases} R_C = F_C - K_{CA}K_{AA}^{-1} F_A \\ R_D = F_D - K_{DB}K_{BB}^{-1} F_B \\ \widetilde{K_{CC}} = K_{CC} - K_{CA}K_{AA}^{-1} K_{AC} \\ \widetilde{K_{DD}} = K_{DD} - K_{DB}K_{BB}^{-1} K_{BD} \end{cases}$$

On solving Eq. (3) and determining $D_C$ and $D_D$, $D_A$ and $D_B$ are next obtained employing Eq. (2). Through this numerical calculation method it is possible to analyze a major dimension matrix calculation as an equivalent minor dimension matrix calculation.

4. Parameter study

In order to study the effect of the contact ratio of the base mat due to embedment depth and bedrock rigidity, analysis was performed with embedment depth and bedrock rigidity as parameters, and along with carrying out comparison studies of the various cases, comparisons of the contact ratios between the precise and conventional methods were made.

4.1 Analysis conditions

The object of analysis is the nuclear reactor building shown in Fig. 6, with plan dimensions of 70 x 70 m and height of 75 m.

The analysis model is a two-dimensional FEM model as shown in Fig. 7, and the structure was modeled to give equivalent rigidity and weight. The domain of the soil was assumed in a range considered as not influencing the analysis of interaction between structure and soil.

The boundary conditions were for the analytical rock base to be fixed, and for side end to be fixed at horizontal direction under vertical load and to be fixed at vertical direction under earthquake load. Further, in analysis under vertical load the method of executing backfilling work was considered, and backfill soil was made to slide along the side of the structure and face of slope.

In vertical load analysis the dead weight of the structure and backfill soil were added as vertical loads (Fig. 8). The earthquake load up to 3 times the design seismic coefficient (corresponding to 0.2 G, hereinafter indicated as 1 K) based on the Japanese Building Code was divided into 30 equal increment load, after which up to 6 times was divided into 60 equal incremental loads. The seismic coefficient distribution for lateral earthquake loads

at the time of 3 K is shown in Fig. 9. However, for the seismic coefficient distribution of lateral earthquake loads of the soil, hypotheses were made referring to the results of dynamic analysis results.

As for shear wave velocity (Vs) of the backfill soil portion, 100 - 200 m/sec was assumed, while for nonlinear springs between the structure and soil, experimental data were referred to and cohesion (C) and angle of friction ($\phi$) between the structure and backfill soil were assumed as 0.28 kg/cm$^2$ and 22°, respectively, while between the structure and bedrock they were assumed to be 0.40 kg/cm$^2$ and 36°.

4.2 Analytical cases

The five analytical cases were chosen as shown in Table 2. The parameters of embedment depth were the three kinds of 0 m, 20 m and 40 m as shown in Fig. 10, while the parameters of bedrock rigidity were the three levels of shear wave velocity (Vs) of 600 m/sec, 1,000 m/sec and 1,500 m/sec.

4.3 Analytical results

The results of analyses are given below focusing on comparisons with the conventional method, influence of embedment depth and influence of bedrock rigidity.

4.3.1 Comparisons with conventional method

Regarding Case 1 (embedment depth 0 m, Vs = 600 m/sec), the state between structure and soil at 4.0 K is shown in Table 3 compared with the conventional method. It can be seen from this table that even when there is no embedment, the contact ratio by the precise analysis method is higher than that by the conventional method due to elastic deformations of soil and structure.

Case 2 (embedment depth 20 m, Vs = 600 m/sec) is described comparing with the conventional method. The contact ratio with the conventional method in the case there is embedment, was obtained determining the overturning moment of the structure by reducing the moment due to axial force of the soil at the side of the structure from the total resisting moment in the analytical results with rock pressures, taken to be of triangular distribution from the overturning moment and the dead weight of the structure.

The bending moment of the structure at 4.5 K and the distribution of shear force in the direction of height are shown in Fig. 11 in comparison with the conventional method. The bending moment of the portion of the structure embedded in soil is smaller than that of for the conventional method, and the effect of frictional resistance of the side surface of the structure is evident.

The gross resisting moment of soil and rock at the contact surface, and the shares of the individual resistance mechanisms of side-surface axial resistance, side-surface frictional resistance and base mat bottom-surface resistance are shown in Fig. 12. The proportion of side-surface frictional resistance in the gross resisting moment is 23% at 4.5 K and 26% at 6.0 K.

The soil pressure distributions at the side and bottom surfaces of the structure at 4.5 K are shown in Fig. 13. The rock pressure distribution at the base mat bottom surface shows concentrations at edges compared with the triangular distribution assumed for the conventional method, which indicates the influence of the soil-structure elastic deformation.

The contact ratio of the base mat compared with the conventional method is shown in Fig. 14. After uplift has occurred, the contact ratio according to the precise analysis method becomes increasingly higher than that of the conventional method. This is estimated

to be the effect of side-surface frictional resistance and elastic deformation of the soil-structure.

4.3.2 Influence of embedment depth

In order to examine the influence of embedment depth on the contact ratio of the base mat, comparison of the contact ratios in the three cases of Case 1 (embedment depth 0 m), Case 2 (embedment depth 20 m) and Case 5 (embedment depth 40 m) was made (Fig. 15). The results indicate that contact ratio becomes higher as embedment depth is increased.

Fig. 16 shows the relation between contact ratios by both method. This figure also shows that the contact ratio by the precise analysis method is considerably higher than that by the conventional method.

4.3.3 Influence of rock excavation

In order to study the influence of bedrock rigidity on the contact ratio of the base mat, comparisons were made of the contact ratios of the three cases of Case 2 (Vs = 600 m/sec), Case 3 (Vs = 1,000 m/sec) and Case 4 (Vs = 1,500 m/sec)(Fig. 17). The results show there is a tendency for contact ratio to become higher when the bedrock rigidity becomes low, and this is thought to be the influence of elastic deformation.

The contact ratios for the three cases are shown in Fig. 18 compared with the conventional method. Here again, the contact ratio by the precise analysis method is higher than by the conventional method.

## 5. Conclusion

The features of this study are that in evaluation of the contact ratio of the base mat of a structure, elastic deformation of the soil-structure system and nonlinearity at the contact surface between the structure and soil were adopted.

As case studies, FEM analyses were performed as parameters of embedment depth and bedrock rigidity, and comparisons were made between cases and with the conventional method, and the following were clarified:

(1) The contact ratio according to the precise analysis method becomes higher than that of the conventional method due to the effects of side-surface frictional resistance and elastic deformations of the structure and soil.

(2) The effect of side-surface frictional resistance becomes remarkable as the depth of embedment increases, and therefore the contact ratio becomes higher.

(3) When the bedrock rigidity becomes low there is a tendency for contact ratio to increase due to the effect of elastic deformation of the bedrock.

This study deals with soil-structure interaction as a static nonlinear problem, but since it is thought that the influences of dynamic effects are also large for problems of this type, this aspect is presently being examined.

## References

(1) D.G. Row and J.G. Powell, "A Substructure Technique for Nonlinear Static and Dynamic Analysis, EERC-78/15.

(2) K. Atsumi and K. Ujiie et al., "Contact Ratio of Base Mat Considering Soil-Structure Nonlinearity", Transactions of the AIJ, 1981 (Part 1 - Part 4), 1982 (Part 5 - Part 7) (in Japanese).

Table 1. Evaluation Method of Contact Ratio of Base Mat

| Factor | Conventional Method (Approximate Calculation) | Precise Analysis Method | Prediction |
|---|---|---|---|
| Elastic Deformations of Soil and Structure | Elastic Deformation Not Considered 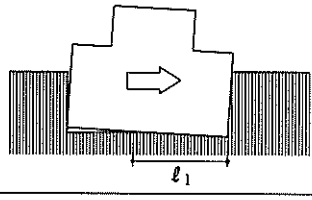  | Elastic Deformation Considered 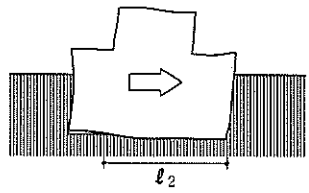  | $\ell_2 > \ell_1$ |
| Resistance of Soil | Resistance of Base Mat 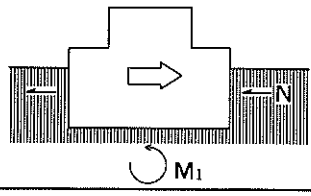  | Resistance of Base Mat<br>Frictional Resistance of External Walls 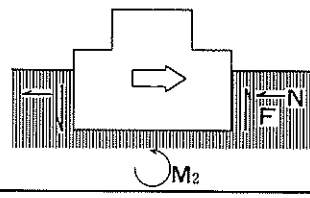  | $M_2 < M_1$<br>$\ell_2 > \ell_1$ |

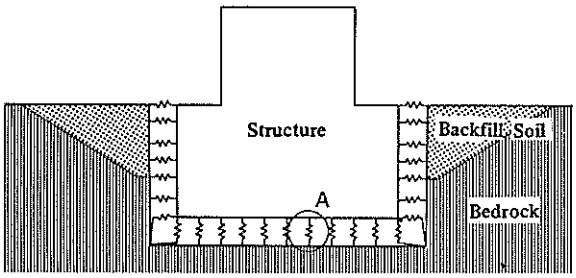


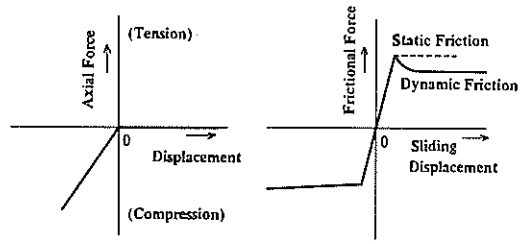


Axial Force-Displacement  Frictional Force-Sliding Displacement

Fig. 1. Force Transmission Mechanism at Boundary

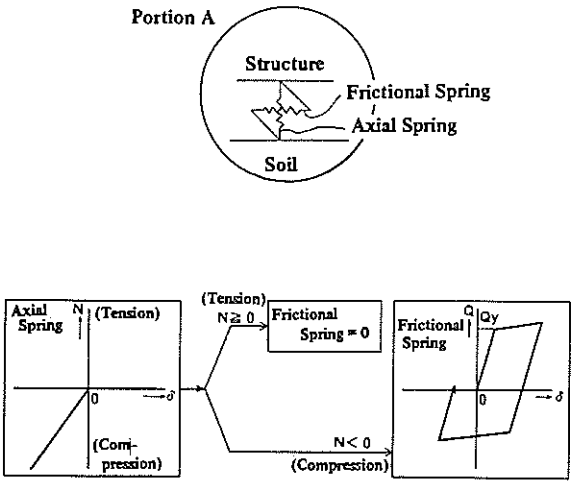


Fig. 2. Nonlinear Springs Between Structure and Soil

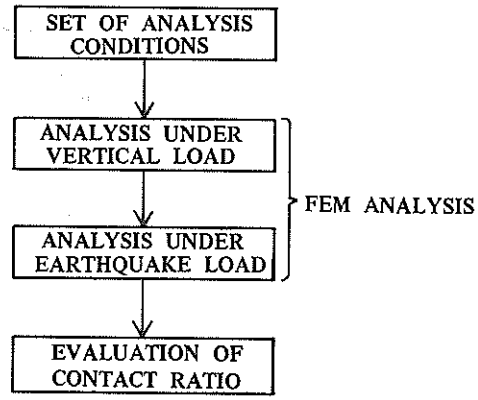


Fig. 3. Flow of Contact Ratio Computation

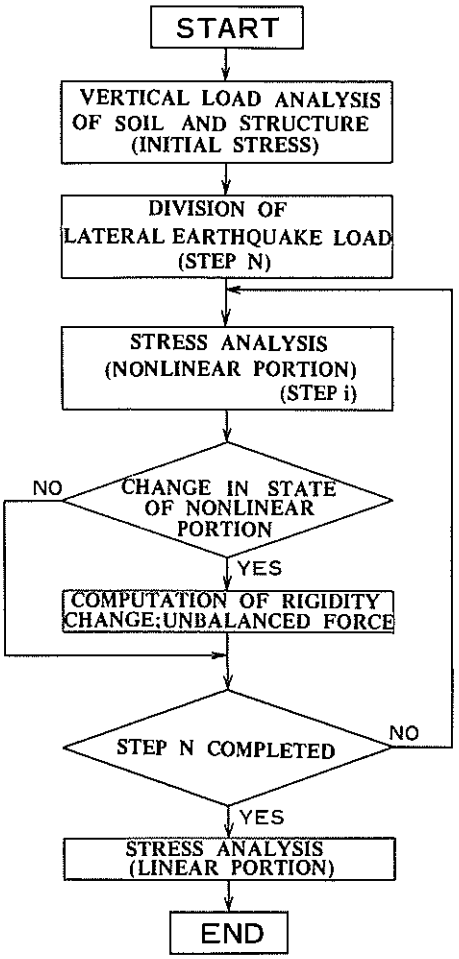


Fig. 4. Flow of Load Increment Method

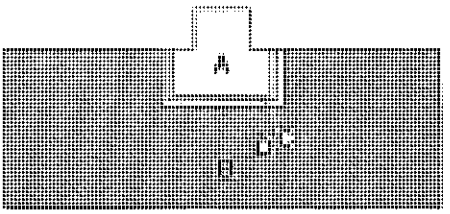


Fig. 5 Division of Analysis Model

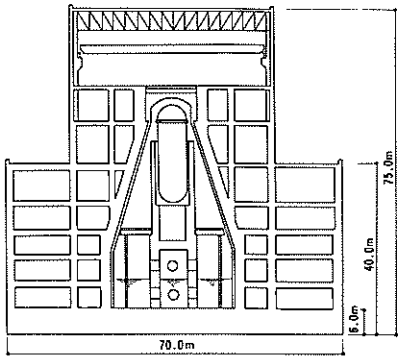


Fig. 6 Model of Nuclear Reactor Building

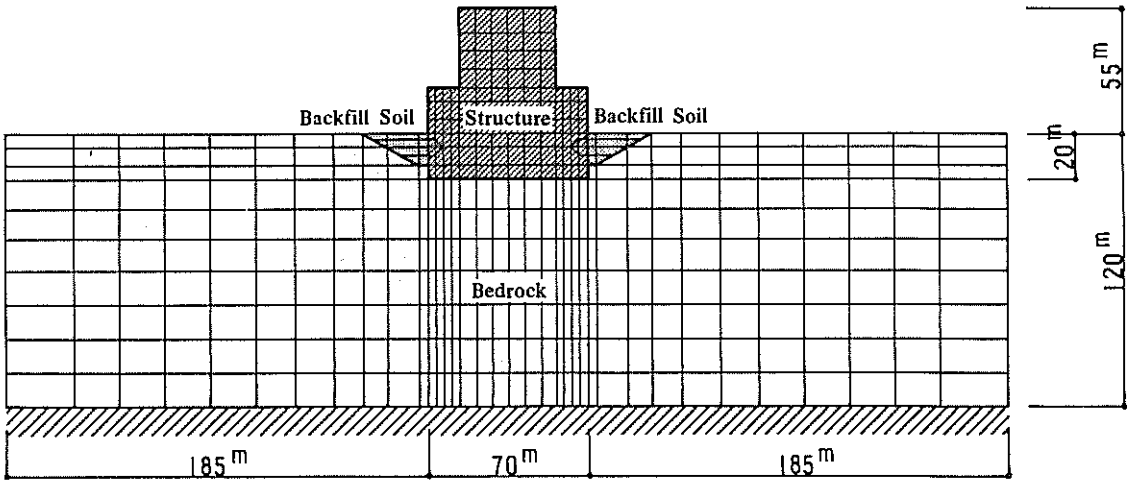


Fig. 7. Analytical Model (Mesh Layout)

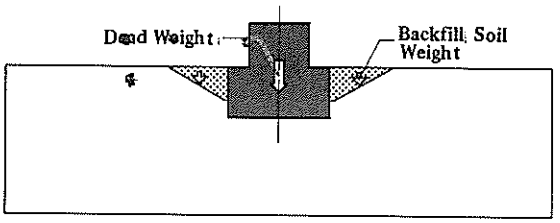


Fig. 8 Vertical Load for Dead Weight Analysis

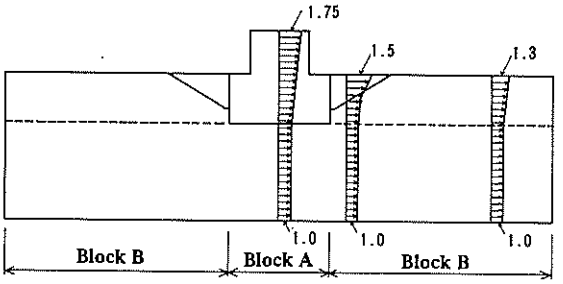


Fig. 9. Seismic Coefficient Distribution For Lateral Earthquake

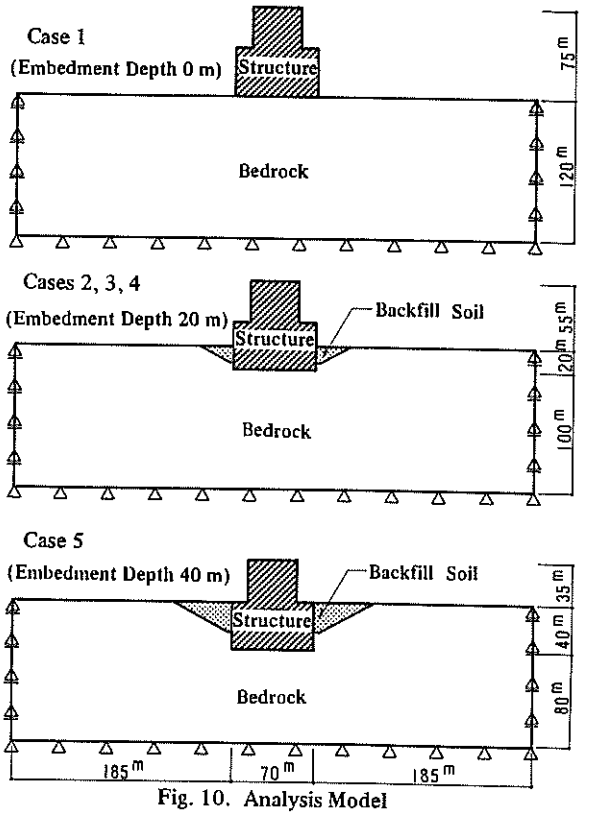


Fig. 10. Analysis Model

Table 2. Analytical Cases

| | Embedment Depth (m) | Shear Wave Velocity of Bedrock (Vs,m/sec) |
|---|---|---|
| Case 1 | 0 | 600 |
| Case 2 | 20 | 600 |
| Case 3 | 20 | 1,000 |
| Case 4 | 20 | 1,500 |
| Case 5 | 40 | 600 |

Table 3. State of Interface (Case 1, 4.0 K)

| Precise Analysis Method | Conventional Method |
|---|---|
| 85 % | 79 % |
| Contact (Elastic Friction) | Contact |
| Contact (Yielded Friction) | |
| Separation | Separation |

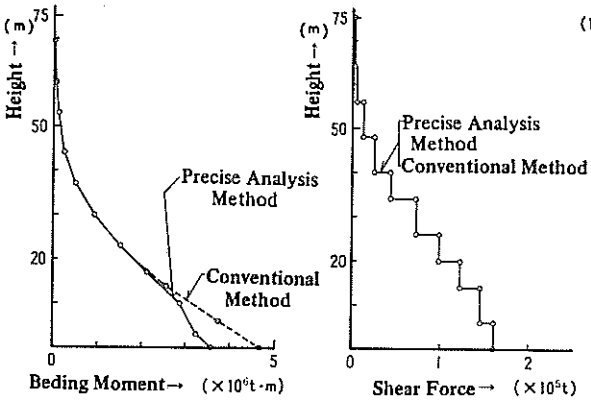


Fig. 11. Seismic Force Distribution of Structure (Case 2, 4.5 K)

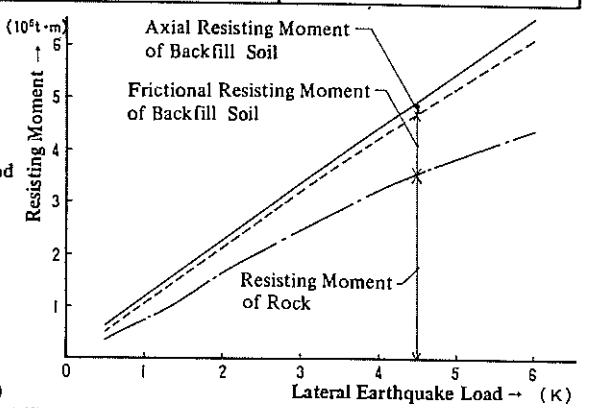


Fig. 12. Constitution of Resisting Moment (Case 2)

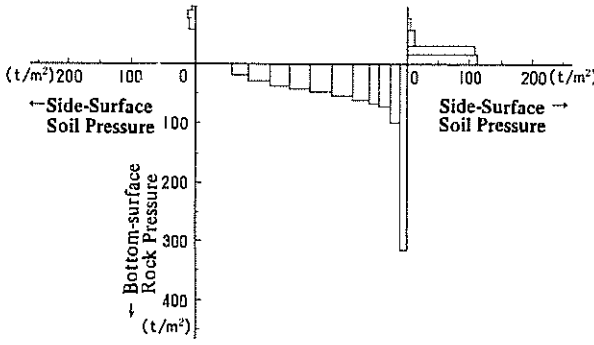


Fig. 13. Soil Pressure Distribution (Case 2, 4.5 K)

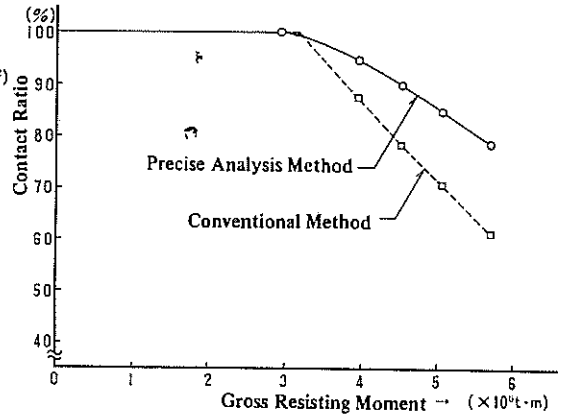


Fig. 14. Comparison with Conventional Method Concerning Contact Ratios (Case 2)

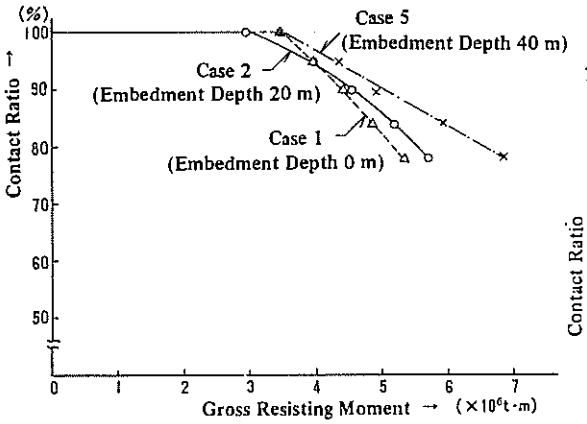


Fig. 15. Comparison of Contact Ratio According to Embedment Depth

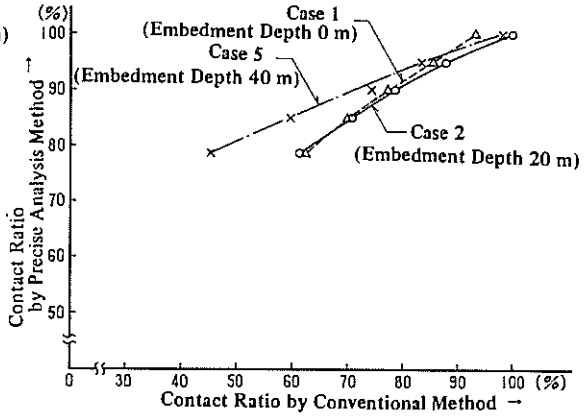


Fig. 16. Comparison with Conventional Method Concerning Contact Ratios

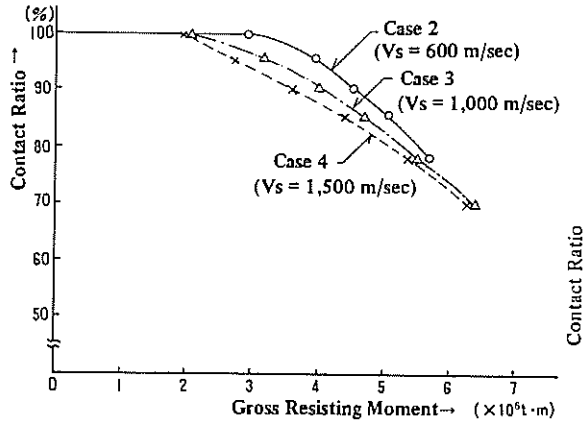


Fig. 17. Comparison of Contact Ratios According to Bedrock Wave Velocity

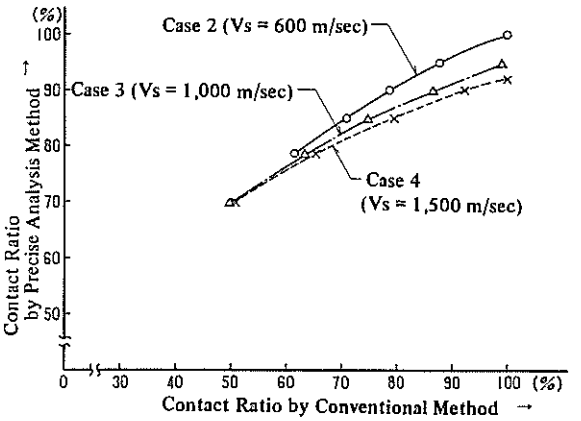


Fig. 18. Comparison with Conventional Method Concerning Contact Ratios